

A systems-level approach to human epileptic seizures – Supplementary material

Christian Rummel^{*,a,1}, Marc Goodfellow^{b,c}, Heidemarie Gast^d, Martinus Hauf^a,
Frédérique Amor^d, Alexander Stibal^e, Luigi Mariani^f, Roland Wiest^a, Kaspar Schindler^d

^a*Support Center for Advanced Neuroimaging (SCAN), Institute of Diagnostic and Interventional
Neuroradiology, Inselspital, Bern University Hospital, University of Bern, Switzerland*

^b*Systems Biology Doctoral Training Centre, Manchester Institute of Biotechnology, The University of
Manchester, Manchester, UK*

^c*Centre for Interdisciplinary Computational and Dynamical Analysis (CICADA), School of Mathematics,
The University of Manchester, Manchester, UK*

^d*qEEG group, Department of Neurology, Inselspital, Bern University Hospital and University of Bern,
Switzerland*

^e*Department of Neurosurgery, Inselspital, Bern University Hospital, University of Bern, Switzerland*

^f*Department of Neurosurgery, Basel University Hospital, University of Basel, Switzerland*

Contents

S1 Multivariate analysis	1
S1.1 Properties of correlation matrices	1
S1.2 Eigenvalues and eigenvectors	1
S2 Supplementary patient examples	3

*Corresponding author

¹Christian Rummel, phone 0041 31 6328038, fax 0041 31 6324872, crummel@web.de

S1. Multivariate analysis

S1.1. Properties of correlation matrices

$M \times M$ correlation matrices \mathbf{CC} and \mathbf{SCC} can be rewritten in quadratic form using the (row-wise normalized) $M \times T$ data matrices $\tilde{\mathbf{X}}$ and $\widetilde{\mathbf{dX}}$ with elements $\tilde{X}_i(t)$ and $\widetilde{\mathbf{dX}}_i(t)$, respectively (row index $i = 1, \dots, M$ and column index $t = 1, \dots, T \gg M$), and the corresponding transposed matrices (denoted by the superscript t):

$$\mathbf{CC} = \frac{1}{T} \tilde{\mathbf{X}} \tilde{\mathbf{X}}^t \quad (\text{S1})$$

$$\mathbf{SCC} = \frac{1}{T-1} \widetilde{\mathbf{dX}} \widetilde{\mathbf{dX}}^t \quad (\text{S2})$$

As a consequence of the basic definitions \mathbf{CC} and \mathbf{SCC} share the following general properties:

$$-1 \leq \mathbf{CC}_{ij} \leq 1 \quad \text{and} \quad -1 \leq \mathbf{SCC}_{ij} \leq 1 \quad (\text{S3})$$

$$\mathbf{CC}_{ii} = 1 \quad \text{and} \quad \mathbf{SCC}_{ii} = 1 \quad (\text{S4})$$

$$\mathbf{CC}_{ji} = \mathbf{CC}_{ij} \quad \text{and} \quad \mathbf{SCC}_{ji} = \mathbf{SCC}_{ij} \quad (\text{S5})$$

S1.2. Eigenvalues and eigenvectors

An $M \times M$ matrix \mathbf{A} with elements A_{ij} (in the context of our paper the $i, j = 1, \dots, M$ denote the artifact-free iEEG channels and the matrix elements the strength of their correlation) describes a linear mapping from M -dimensional vectors \mathbf{v} onto M -dimensional vectors \mathbf{v}' :

$$\mathbf{A} \mathbf{v} = \mathbf{v}' \quad (\text{S6})$$

In general \mathbf{v}' differs from \mathbf{v} in length (norm) and orientation in the M -dimensional space. However, vectors exist that are mapped onto themselves and only their length is changed (by a factor λ):

$$\mathbf{A} \mathbf{v} = \lambda \mathbf{v} \quad (\text{S7})$$

Vectors \mathbf{v}_l that solve this equation point to characteristic directions of the mapping \mathbf{A} . These vectors are called “eigenvectors” and the corresponding factors λ_l are “eigenvalues”. For the special case of cross-correlation matrices of EEG signals, complementary illustrative explanations of eigenvalues and eigenvectors are given in (Schindler et al., 2007b,a; Müller et al., 2008b; Schindler et al., 2010).

General results of linear algebra prove that the eigenvalues of real symmetric matrices ($A_{ji} = A_{ij} \in \mathbb{R}$) are real numbers $\lambda_l \in \mathbb{R}$. They can therefore be given a natural order $\lambda_1 \leq \lambda_2 \leq \dots \leq \lambda_M$. If the matrix \mathbf{A} can be written as a quadratic form (see eq. (S1) and (S2)) the eigenvalues are in addition strictly non-negative $\lambda_l \geq 0$ ($l = 1, \dots, M$).

Matrices with this property are referred to as “positive semi-definite”. Finally, the sum of the eigenvalues is identical to the sum of the diagonal matrix elements: $\sum_{l=1}^M \lambda_l = \sum_{l=1}^M A_{ll}$ (“conservation of the trace”). For the matrices **CC** and **SCC** these general results confine the eigenvalues to the interval $0 \leq \lambda_l \leq M$ and $\sum_{l=1}^M \lambda_l = M$. The eigenvectors \mathbf{v}_l of real symmetric matrices have real components $v_{il} \in \mathbb{R}$ quantifying how \mathbf{v}_l is oriented in the direction of channel “ i ”. Eigenvectors can be normalized to $\sum_{i=1}^M v_{il}^2 = 1$ without loss of generality.

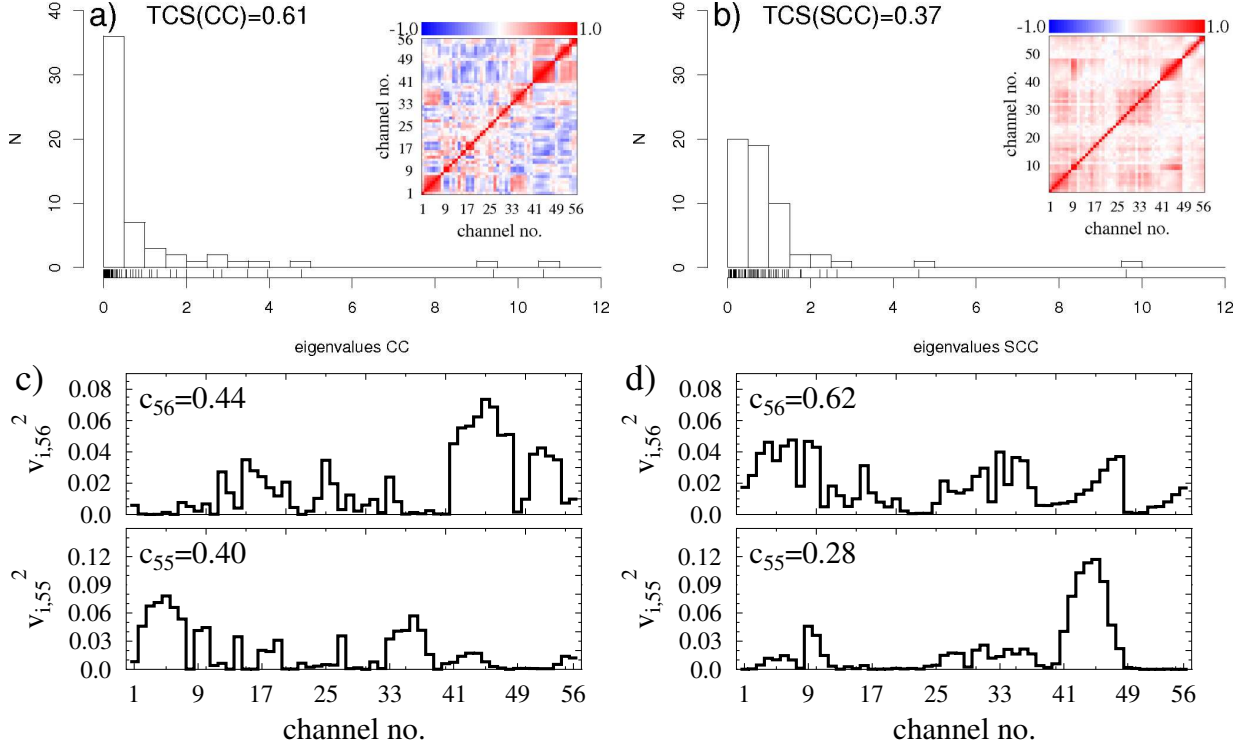


Figure S1: (colour) Comparison of CC (left) and SCC (right) for pre-ictal iEEG data recorded from patient 3. Panels a and b show examples of the matrices and histograms of the corresponding eigenvalue spectra for $M = 56$ and $T = 2048 = 2$ s. Panels c and d show the squared eigenvector components of the two largest eigenvalues. Sequence of iEEG electrodes: left temporo-polar strip electrode (channels 1–8), left temporo-lateral-basal strip electrode (channels 9–16), left fronto-central-temporal strip electrode (channels 17–24), left fronto-orbital strip electrode (channels 25–32), left fronto-polar strip electrode (channels 33–40), left depth electrode (channels 41–48), right depth electrode (channels 49–56).

In Fig. S1 we compare the matrices **CC** (panels a and c) and **SCC** (panels b and d) calculated from a two second window ($T = 2048$) of pre-ictal iEEG data. Panels a and b show an example of the complete matrices and a histogram of the eigenvalue density. The matrix **CC** contains much more anti-correlation (blue shades) and larger average matrix elements than the matrix **SCC**. As a consequence the eigenvalue distribution is more skew and the total correlation strength TCS (see (Müller et al., 2008a) and eq. (5) of the main text) is larger for **CC**.

The squared components v_{il}^2 of the eigenvectors corresponding to the two largest eigenvalues (abbreviated as “largest eigenvectors” henceforth) of the matrices **CC** and **SCC** are displayed in panels c and d. They give information regarding the extent to which channel “ i ” is involved in eigenvector \mathbf{v}_l . The largest eigenvector of the matrix **SCC** reveals the most collective behavior ($c_{56} = 0.62$, see (Plerou et al., 2002) and eq. (6) of the main text) and the separation of collectivity from the second largest eigenvector ($c_{55} = 0.28$) is much larger than for the matrix **CC** ($c_{56} = 0.44$ and $c_{55} = 0.40$).

The M eigenvectors \mathbf{v}_l of correlation matrices provide spatial information regarding the contribution of EEG channels to correlation patterns. Recently, eigenvectors of correlation and synchronization matrices and vectors derived from them have been applied for data clustering (Bialonski and Lehnertz, 2006; Allefeld et al., 2007; Rummel et al., 2007; Allefeld and Bialonski, 2007; Rummel, 2008; Rummel et al., 2008). The common background to these approaches is that the dominant components of a small group of large eigenvectors represent hypercorrelated subgroups (“clusters”). Typically, random and inter-cluster correlations are not negligible. In such situations the largest eigenvector \mathbf{v}_M has sizable contributions from *all* channels taking part in at least one cluster (see e.g. Figs. 1 of (Rummel et al., 2007; Rummel, 2008)). In the M -dimensional space spanned by the iEEG signals \mathbf{v}_M points to the direction of largest variance, cf. Principal Component Analysis (PCA, Jolliffe (1986)). In order to infer the highly correlated channels without specifying to which cluster they belong, this feature allows one to concentrate on the M components v_{iM} of the largest eigenvector \mathbf{v}_M as opposed to the much larger number of $M(M-1)/2$ independent matrix elements A_{ij} of symmetric correlation matrices. In the present study we followed this simplification.

S2. Supplementary patient examples

In this section we present compilations of peri-ictal dynamics of eigenvalue and eigenvector based quantifiers for the first seizure of all patients. Results are given for both **SCC** and **CC**. TCS and collectivity behave similarly for both matrices in most cases. In contrast, the fluctuations of the largest eigenvectors as measured by the scalar product with the template vector (see eq. (7) of the main text) are often much larger for **CC** than for **SCC**. As a consequence, eigenvector excess and depletion are meaningful only for **SCC** in most cases.

The first seizure of patient 1 is discussed as an example in which the first ictal changes consist of local **SCC** eigenvector *excess* rather than depletion. Patient 6 suffered from seizures starting in the right *and* the left hemisphere. The first seizure of either category is discussed.

In Fig. S2 we present the example of **seizure 1 of patient 1**. Similarly to the results of Fig. 4a of the main text TCS increases during seizure (panel a). In this case, the epileptiform activity terminates when TCS has reached its maximal value (panel d). The collectivity increases after seizure onset, then decreases and finally strongly fluctuates at an elevated level after seizure termination (panel b). The scalar product with the template vector shows the opposite behavior (panel c). Comparison of panels d and e reveals a significant change of the pattern of the largest eigenvector of the matrix **SCC** two minutes before visual seizure onset and before epileptiform activity is present on any of the iEEG channels. In contrast to the majority of cases, here the first change consists of a significant local eigenvector *excess* of the left foramen ovale electrodes (channels 1 and 2) and to a lesser extent of the right temporo-anterior contact 20. Note also that for this seizure the channels showing early epileptiform activity (SOZ) are identical to the channels showing first ictal eigenvector *depletion* (right temporo-anterior strip electrode, channels 19–26). For this seizure the onset times of epileptiform activity and eigenvector depletion are correlated with only marginal significance ($r_{sd} = 0.377$, $p_{sd} = 0.028$) and anti-correlation with eigenvector excess is insignificant ($r_{sx} = -0.271$, $p_{sx} = 0.121$). Significance of these correlations is improved for seizures 2–4 of this patient, where temporal stability of the scalar product between eigenvector and template vector is also larger (Fig. 5 of the main text). Interestingly, for seizure 1 of patient 1 most of the surgically removed tissue (channels 19–26) shows early ictal (and post-ictal) eigenvector depletion but no eigenvector excess. The pattern of dynamical eigenvector excess and depletion of the matrix **SCC** (Fig. S2e) is similar to the peri-ictal rearrangement of the largest eigenvector of a different correlation measure for the same data, which was employed to obtain Fig. 5d of (Rummel et al., 2010). Note that in contrast to the previous measure, SCC does not require iterative surrogate generation and is therefore computationally much more efficient.

The behavior of TCS calculated from the eigenvalues of the matrix **CC** (Fig. S3) resembles that derived from **SCC**. In contrast, fluctuations are much larger for the eigenvector based quantities of collectivity and scalar product. As a consequence, significant eigenvector excess and depletion with respect to the pre-ictal reference segment are almost absent for **CC**.

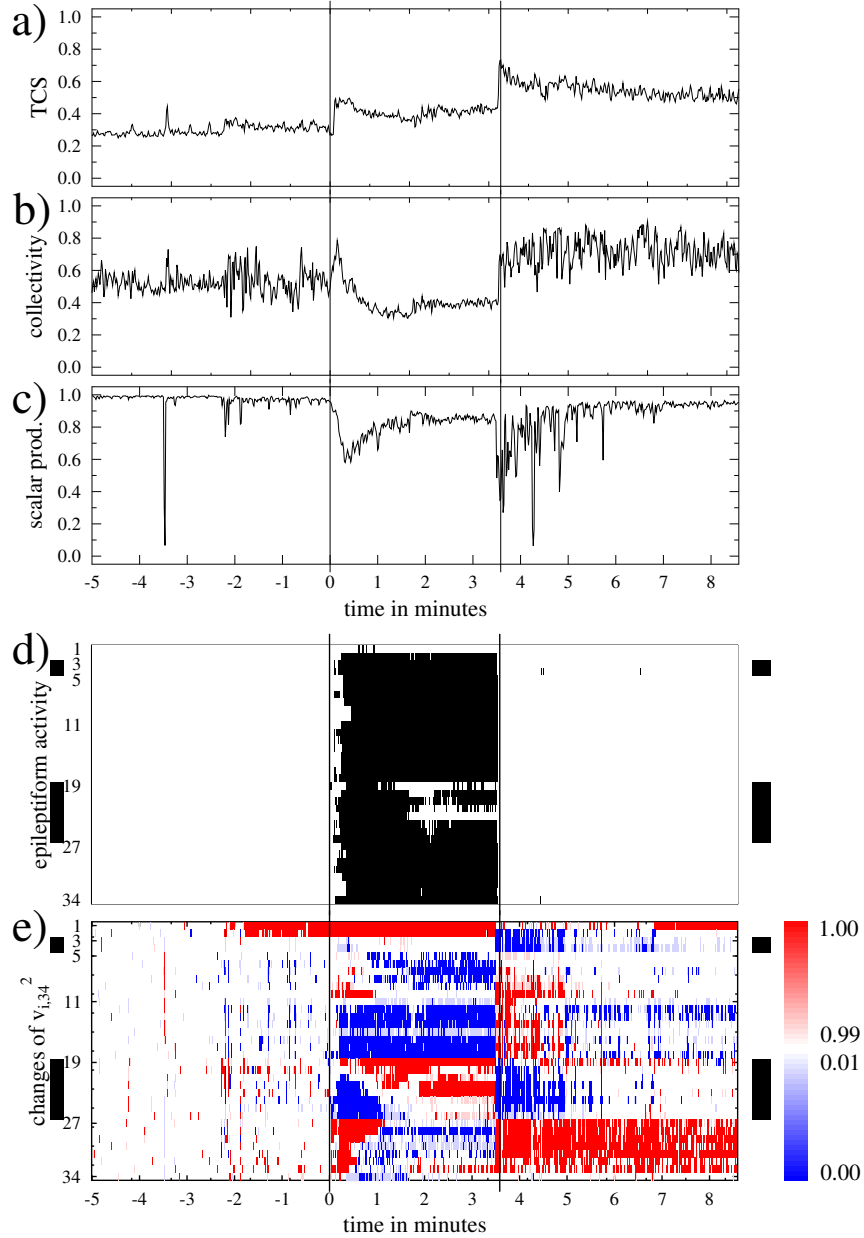


Figure S2: (colour) Temporal evolution of measures derived from the **SCC** matrix during the **first seizure of patient 1**. a) total correlation strength (TCS), b) collectivity of the largest eigenvector, c) scalar product of largest eigenvector with template vector, d) epileptiform activity (epileptiform: black, normal: white), e) significant depletion (blue) and excess (red) of local hypercorrelation as assessed by the squared components of the largest eigenvector of the matrix **SCC**. Sequence of iEEG channels from top to bottom: left foramen ovale electrodes (channels 1, 2), right foramen ovale electrodes (channels 3, 4), right temporo-polar strip electrode (channels 5–10), right temporo-basal strip electrode (channels 11–18), right temporo-anterior strip electrode (channels 19–26), right occipital strip electrode (channels 27–34). Visually defined seizure onset and termination are marked with fully drawn vertical lines. Channels recording from regions that were later surgically removed are marked by bars on the left and right margins of panels d and e.

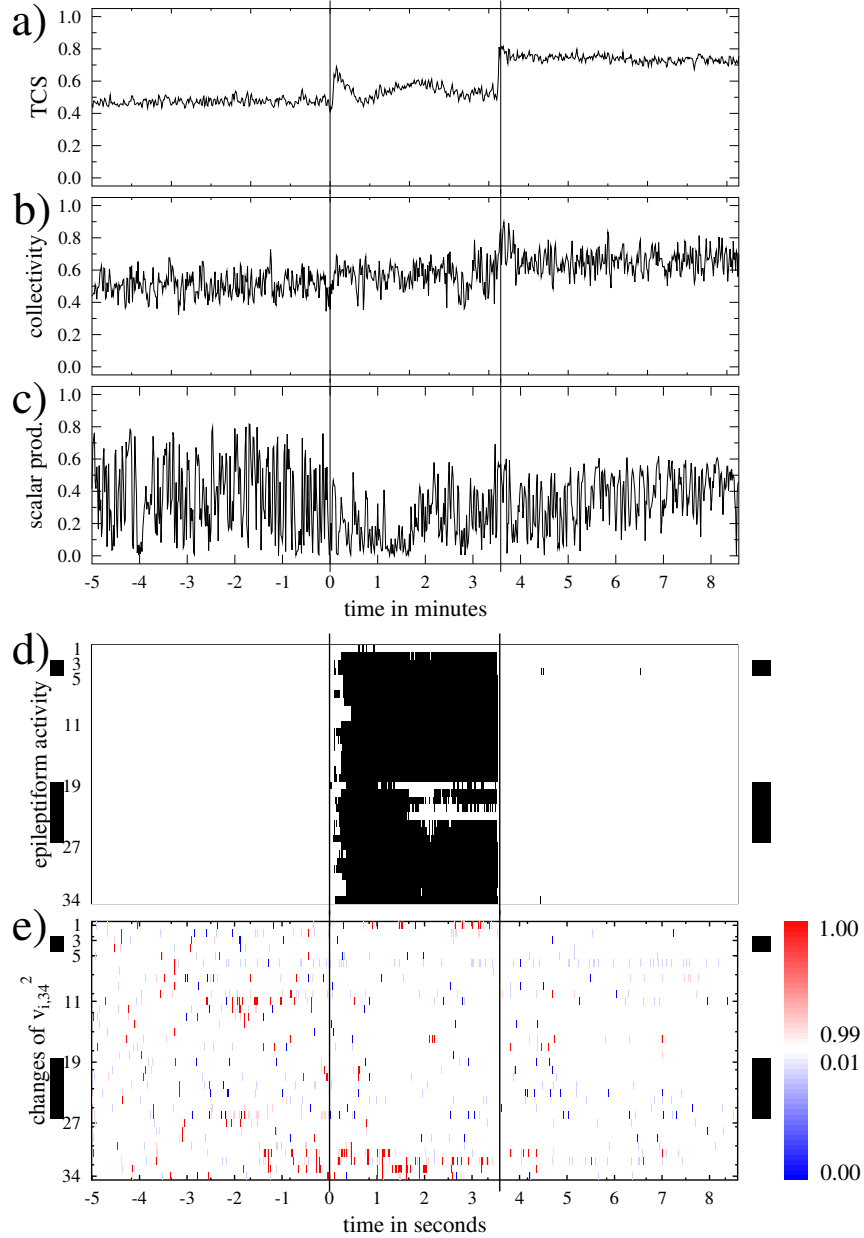


Figure S3: (colour) Same as Fig. S2 but for **CC** based measures for the **first seizure of patient 1**. Sequence of iEEG channels from top to bottom: left foramen ovale electrodes (channels 1, 2), right foramen ovale electrodes (channels 3, 4), right temporo-polar strip electrode (channels 5–10), right temporo-basal strip electrode (channels 11–18), right temporo-anterior strip electrode (channels 19–26), right occipital strip electrode (channels 27–34). Channels recording from regions that were later surgically removed are marked by bars on the left and right margins of panels d and e.

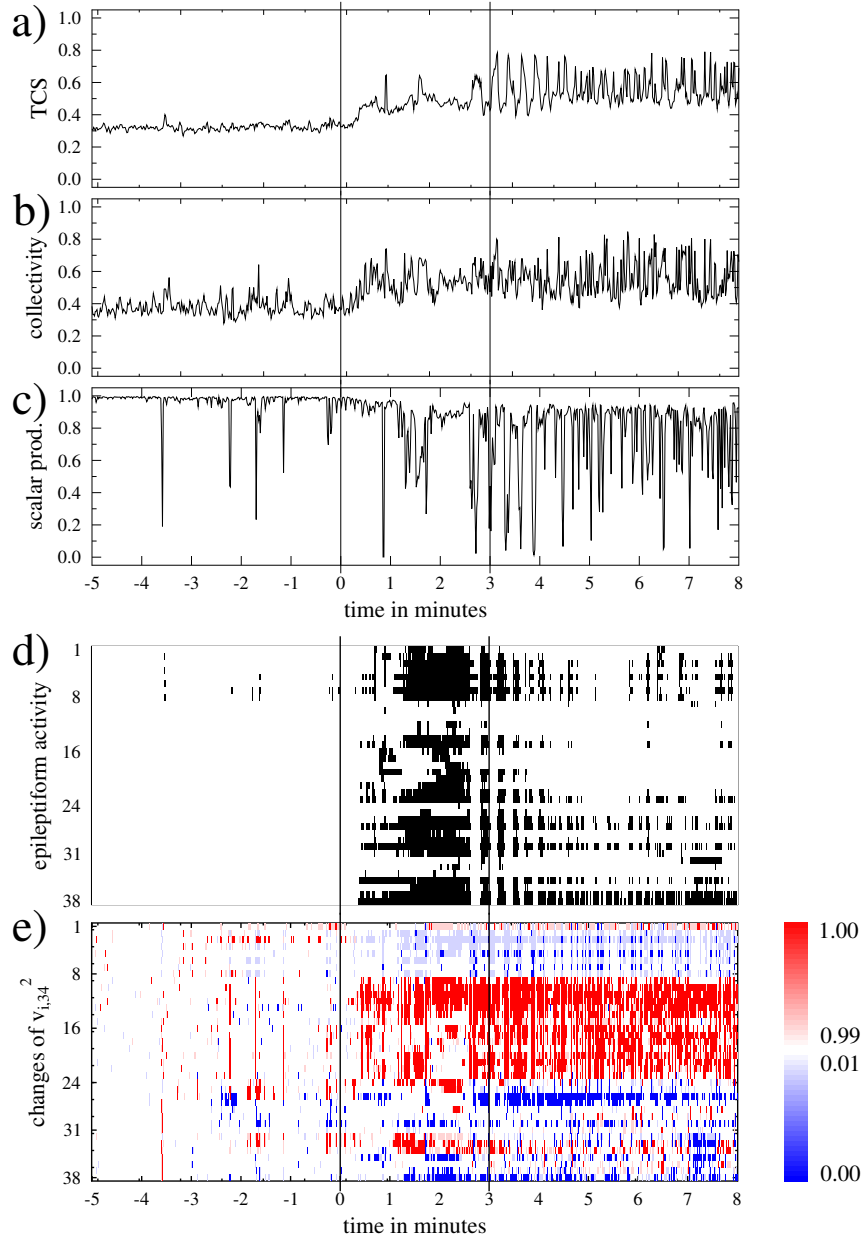


Figure S4: (colour) Same as Fig. S2 but for **SCC** based measures for the **first seizure of patient 2**. Sequence of iEEG channels from top to bottom: foramen ovale electrodes (channels 1, 3, 5, 7 record from the left and channels 2, 4, 6, 8 from the right mesial temporal lobe), left fronto-polar strip electrode (channels 9–15), left fronto-latero-basal strip electrode (channels 16–23), two left temporo-lateral strip electrodes (channels 24–31 and 32–38).

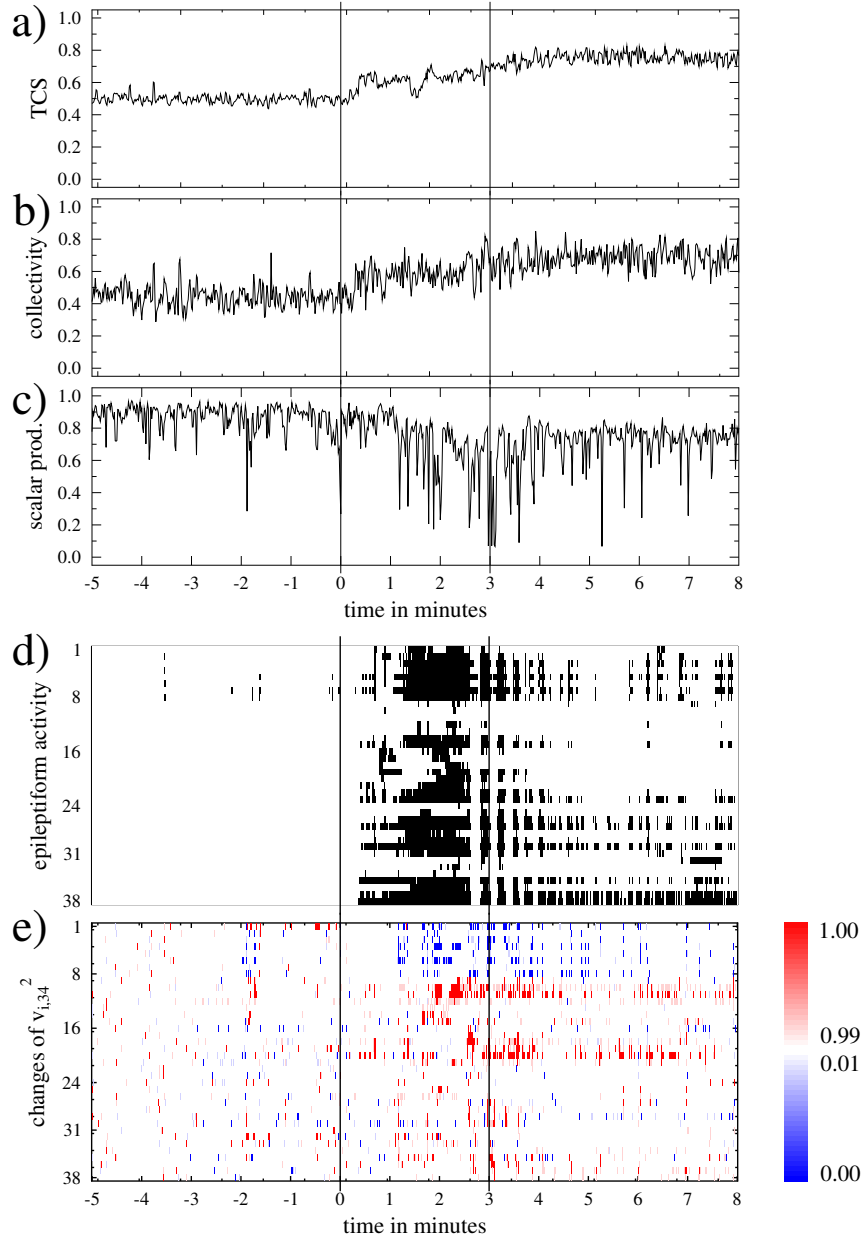


Figure S5: (colour) Same as Fig. S4 but for **CC** based measures for the **first seizure of patient 2**. Sequence of iEEG channels from top to bottom: foramen ovale electrodes (channels 1, 3, 5, 7 record from the left and channels 2, 4, 6, 8 from the right mesial temporal lobe), left fronto-polar strip electrode (channels 9–15), left fronto-latero-basal strip electrode (channels 16–23), two left temporo-lateral strip electrodes (channels 24–31 and 32–38).

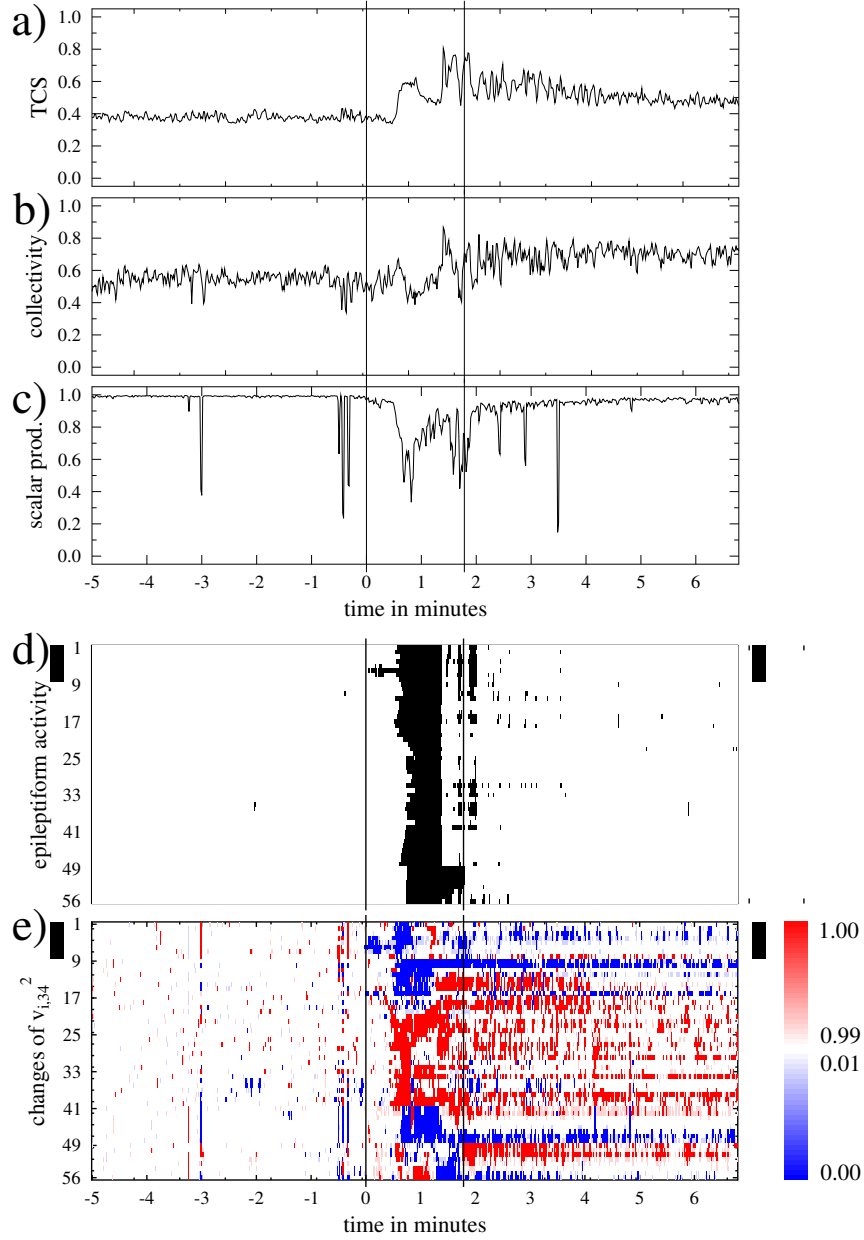


Figure S6: (colour) Same as Fig. S2 but for **SCC** based measures for the **first seizure of patient 3**, cf. Figs. 3 and 4 of the main text where the second seizure is shown. Sequence of iEEG channels from top to bottom: left temporo-polar strip electrode (channels 1–8), left temporo-lateral-basal strip electrode (channels 9–16), left fronto-central-temporal strip electrode (channels 17–24), left fronto-orbital strip electrode (channels 25–32), left fronto-polar strip electrode (channels 33–40), left depth electrode (channels 41–48), right depth electrode (channels 49–56). Channels recording from regions that were later surgically removed are marked by bars on the left and right margins of panels d and e.

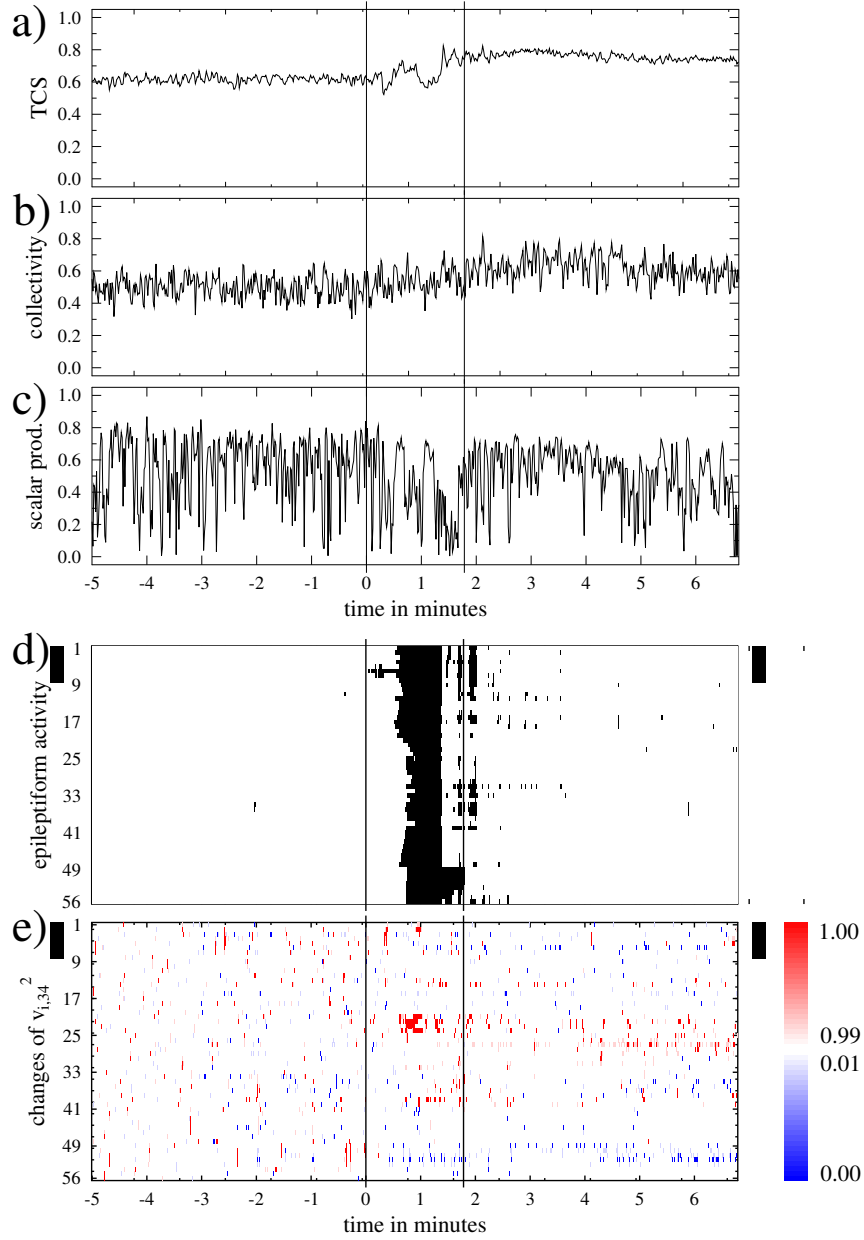


Figure S7: (colour) Same as Fig. S2 but for **CC** based measures for the **first seizure of patient 3**. Sequence of iEEG channels from top to bottom: left temporo-polar strip electrode (channels 1–8), left temporo-lateral-basal strip electrode (channels 9–16), left fronto-central-temporal strip electrode (channels 17–24), left fronto-orbital strip electrode (channels 25–32), left fronto-polar strip electrode (channels 33–40), left depth electrode (channels 41–48), right depth electrode (channels 49–56). Channels recording from regions that were later surgically removed are marked by bars on the left and right margins of panels d and e.

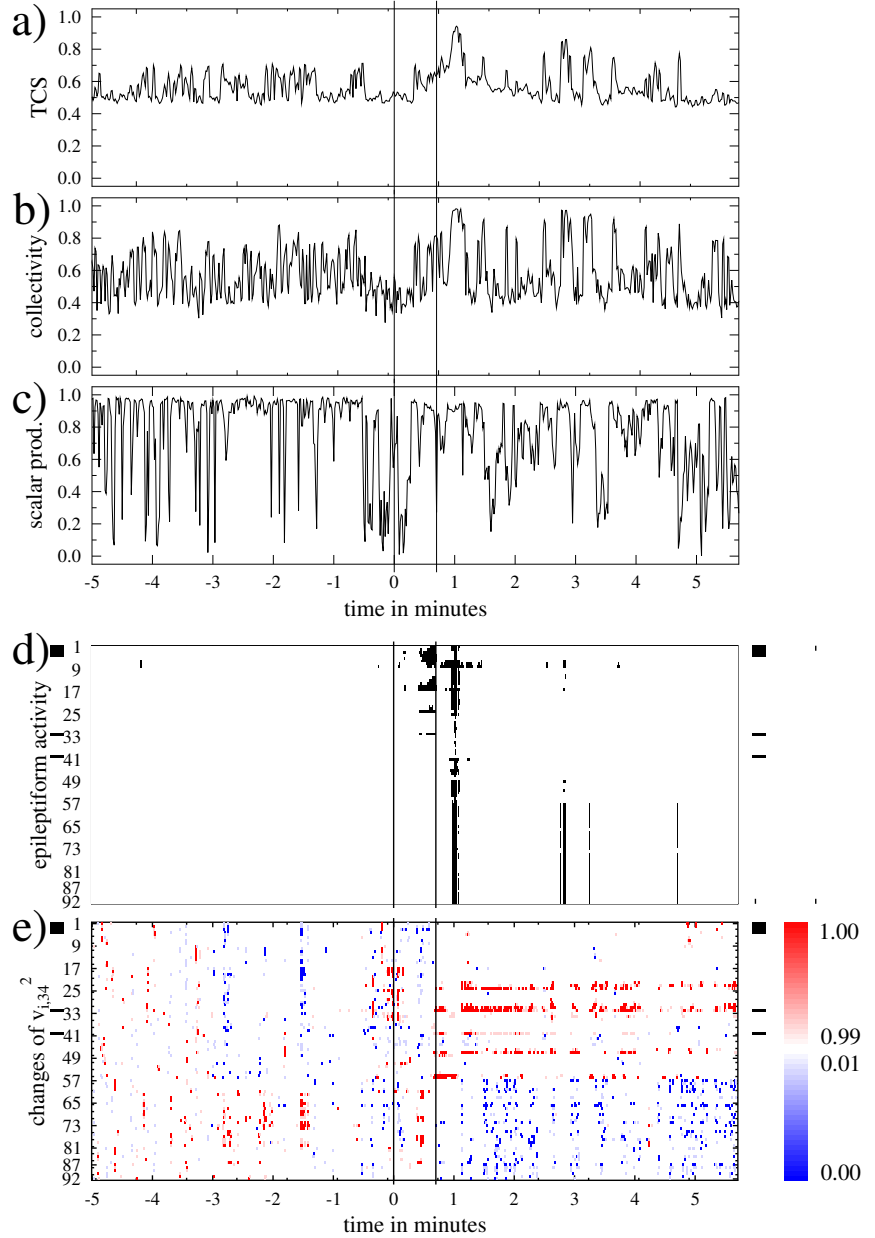


Figure S8: (colour) Same as Fig. S2 but for **SCC** based measures for the **first seizure of patient 4**. Sequence of iEEG channels from top to bottom: right parieto-central depth electrode (channels 1–8), right fronto-orbital depth electrode (channels 9–16), right fronto-parieto-central strip electrode (channels 17–24), right right fronto-dorso-lateral strip electrode (channels 25–32), right fronto-orbital strip electrode (channels 33–40), right fronto-temporal strip electrode (channels 41–48), left fronto-parieto-central strip electrode (channels 49–56), left fronto-dorso-lateral strip electrode (channels 57–64), left fronto-orbital strip electrode (channels 65–72), left fronto-temporal strip electrode (channels 73–80), right fronto-interhemispheric strip electrode (channels 81–86), left fronto-interhemispheric strip electrode (channels 87–92). Channels recording from regions that were later surgically removed are marked by bars on the left and right margins of panels d and e.

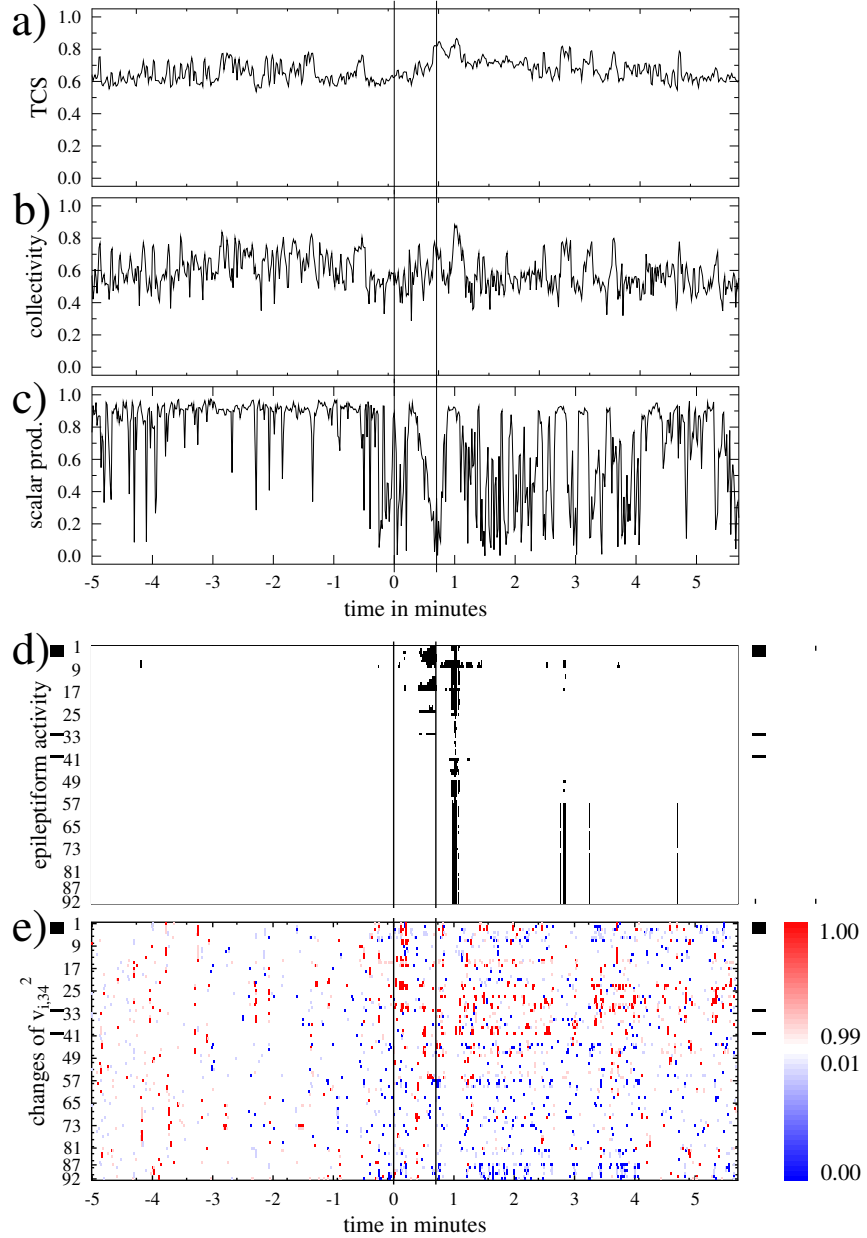


Figure S9: (colour) Same as Fig. S8 but for **CC** based measures for the **first seizure of patient 4**. Sequence of iEEG channels from top to bottom: right parieto-central depth electrode (channels 1–8), right fronto-orbital depth electrode (channels 9–16), right fronto-parieto-central strip electrode (channels 17–24), right right fronto-dorso-lateral strip electrode (channels 25–32), right fronto-orbital strip electrode (channels 33–40), right fronto-temporal strip electrode (channels 41–48), left fronto-parieto-central strip electrode (channels 49–56), left fronto-dorso-lateral strip electrode (channels 57–64), left fronto-orbital strip electrode (channels 65–72), left fronto-temporal strip electrode (channels 73–80), right fronto-interhemispheric strip electrode (channels 81–86), left fronto-interhemispheric strip electrode (channels 87–92). Channels recording from regions that were later surgically removed are marked by bars on the left and right margins of panels d and e.

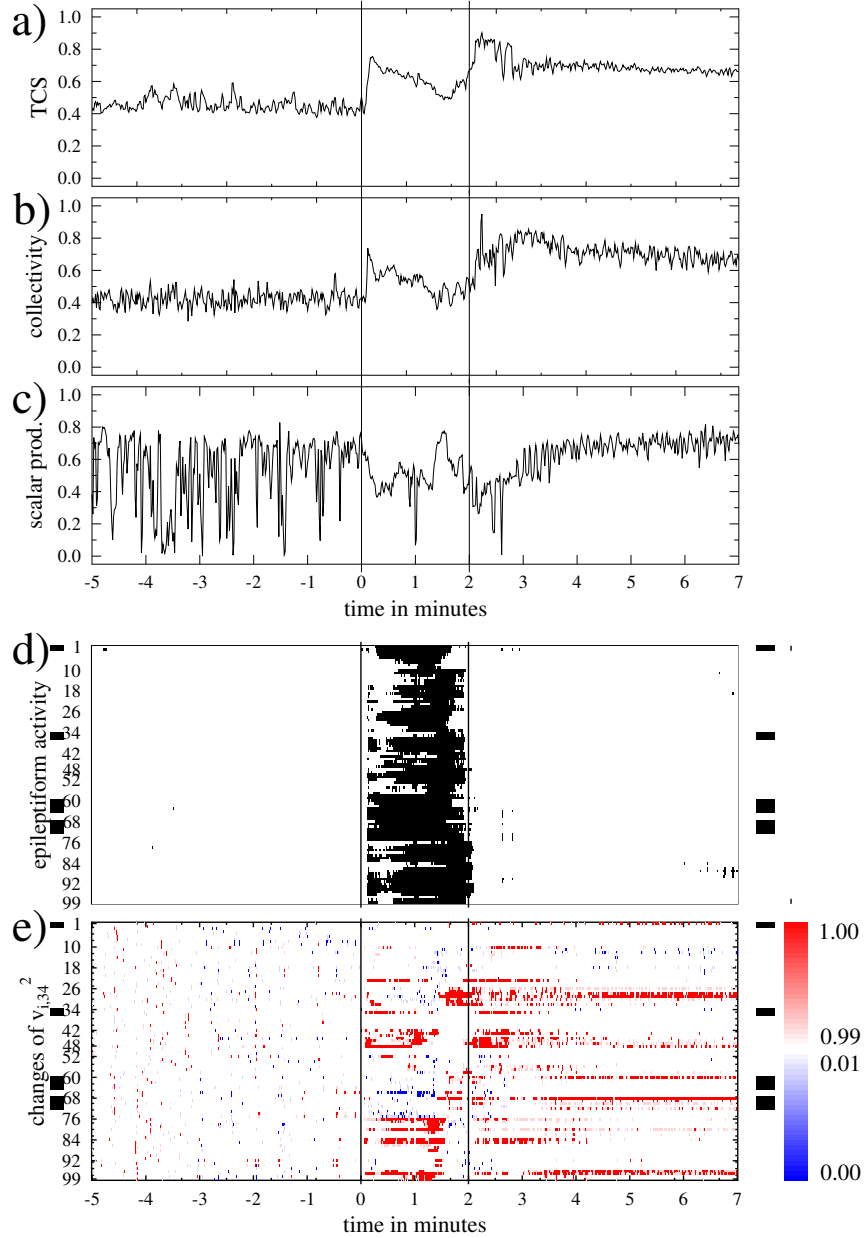


Figure S10: (colour) Same as Fig. S2 but for **SCC** based measures for the **first seizure of patient 5**. Sequence of iEEG channels from top to bottom: depth electrode in the right amygdala (channels 1–10), right fronto-dorso-lateral strip electrode (channels 11–18), right fronto-orbital strip electrode (channels 19–26), right fronto-temporal strip electrode (channels 27–34), right fronto-polar strip electrode (channels 35–42), right anterior interhemispheric strip electrode (channels 43–48), right posterior interhemispheric strip electrode (channels 49–52), right temporo-fronto-orbital strip electrode (channels 53–60), right temporo-basal strip electrode (channels 61–68), right temporo-polar strip electrode (channels 69–76), left fronto-polar strip electrode (channels 77–84), left fronto-dorso-lateral strip electrode (channels 85–92), left fronto-orbital strip electrode (channels 93–99). Channels recording from regions that were later surgically removed are marked by bars on the left and right margins of panels d and e.

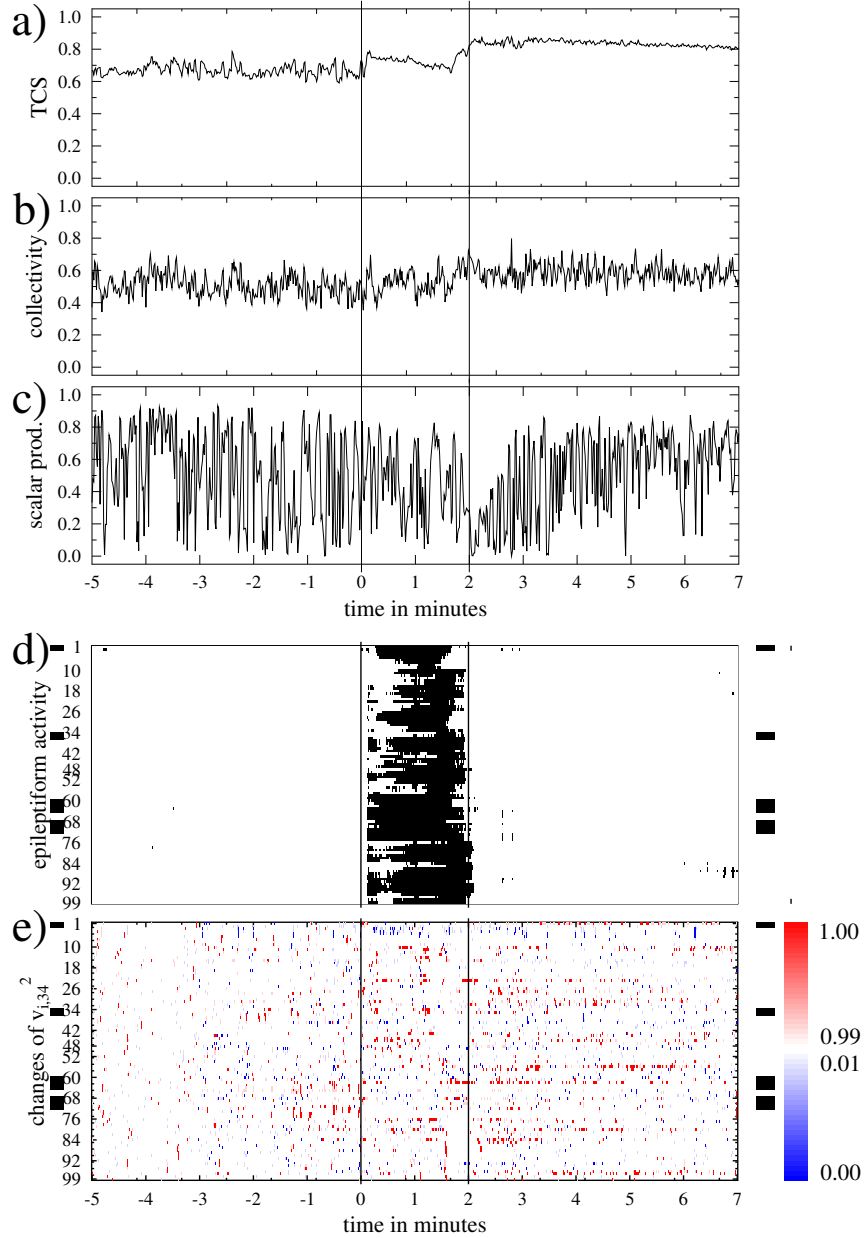


Figure S11: (colour) Same as Fig. S10 but for **CC** based measures for the **first seizure of patient 5**. Sequence of iEEG channels from top to bottom: depth electrode in the right amygdala (channels 1–10), right fronto-dorso-lateral strip electrode (channels 11–18), right fronto-orbital strip electrode (channels 19–26), right fronto-temporal strip electrode (channels 27–34), right fronto-polar strip electrode (channels 35–42), right anterior interhemispheric strip electrode (channels 43–48), right posterior interhemispheric strip electrode (channels 49–52), right temporo-fronto-orbital strip electrode (channels 53–60), right temporo-basal strip electrode (channels 61–68), right temporo-polar strip electrode (channels 69–76), left fronto-polar strip electrode (channels 77–84), left fronto-dorso-lateral strip electrode (channels 85–92), left fronto-orbital strip electrode (channels 93–99). Channels recording from regions that were later surgically removed are marked by bars on the left and right margins of panels d and e.

In Figs. S12 to S15 results are shown for **two seizures of patient 6**. This patient suffered from focal, complex-partial as well as rare secondarily generalized seizures. Results for **seizure R01** with onset in the *right* mesio-polar area are displayed in Figs. S12 and S13. For **SCC**, TCS (panel a) and collectivity (panel b) clearly increase during seizure, while the scalar product with the template vector (panel c) decreases. The scalar product almost recovers to the pre-seizure value at seizure termination. In contrast, the elevated TCS and collectivity persist further into the post-ictal period. Panel d shows the epileptiform activity, which starts in the iEEG channels 1–3, 13, 14, 39 and 40 (all recording from the right mesio-polar temporal lobe) and then propagates to almost all channels. In panel e significant local deviations of the squared eigenvector components v_{iM}^2 from the reference segment are shown. Similarly to patient 3 (Fig. 3 of the main text as well as Fig. S6), early epileptiform activity is correlated with significant depletion and anti-correlated with significant excess of the components of the largest **SCC** eigenvector ($r_{sd} = 0.492$, $p_{sd} < 10^{-6}$ and $r_{sx} = -0.608$, $p_{sx} < 10^{-10}$, see Fig. 5 of the main text for all seizures). Surgery for patient 6 consisted of removing the right mesio-polar structures and led to seizure freedom for more than one and a half years. The contacts recording from tissue that was later removed are marked by bars in panels d and e. We also find good agreement between the location of channels showing early epileptiform activity, channels with early eigenvector depletion and channels associated with resected tissue in patients 1 and 3.

In Figs. S14 and S15 the same quantities are shown for **seizure L01** of the same patient with onset in the *left* mesio-temporal area. For **SCC**, variations of TCS, collectivity and the scalar product during seizure are much smaller here than in Fig. S12. With the exception of channels 57–59, which record from the right mesial temporal lobe, the epileptiform activity and local **SCC** eigenvector depletion remain largely confined to a few contacts of the depth electrode implanted into the left hippocampus (channels 19–26) and a strip electrode on the left mesial temporal lobe (channels 79–86), i.e. tissue that was *not* surgically removed. Correlation between onset times of local eigenvector depletion and epileptiform activity is highly significant for all seizures of this type, whereas anti-correlation with local eigenvector excess is insignificant (see Fig. 5 of the main text). After undergoing surgery this patient still suffers rare auras, presumably originating from the left mesio-temporal area active during this type of seizure.

As found in analyses of data from other patients, eigenvector based quantities are much less stable for the **CC** matrix in this case (Figs. S13 and S15), which hinders a meaningful interpretation of eigenvector excess and depletion.

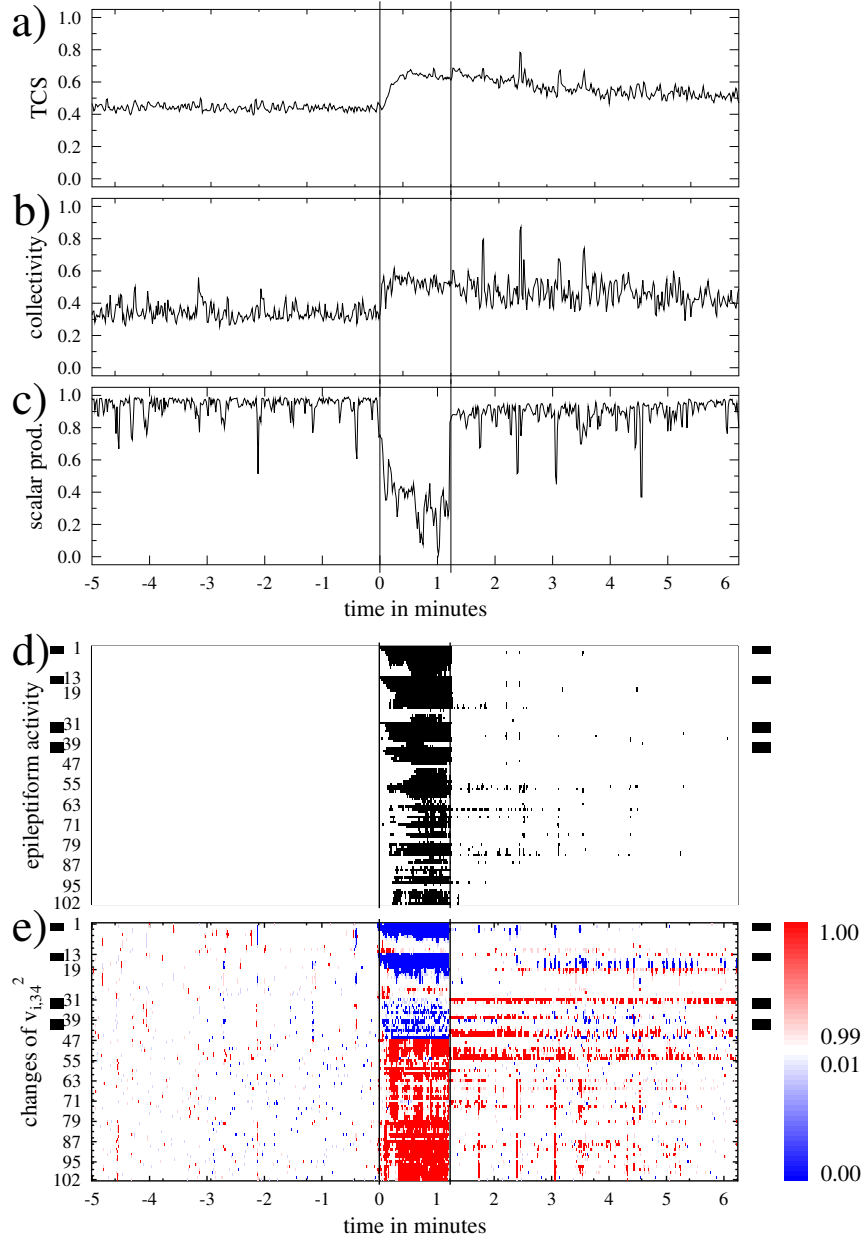


Figure S12: (colour) Same as Fig. S2 but for **SCC** based measures for the **first seizure of patient 6** with onset in the *right* temporal lobe. Sequence of iEEG channels from top to bottom: right temporal depth electrode 1 (channels 1–12), right temporal depth electrode 2 (channels 13–18), left temporal depth electrode (channels 19–30), right temporo-polar strip electrode (channels 31–38), right temporo-basal strip electrode (channels 39–46), right temporo-central strip electrode (channels 47–54), right fronto-mesial strip electrode (channels 55–62), right fronto-polar strip electrode (channels 63–70), right fronto-basal strip electrode (channels 71–78), left fronto-mesial strip electrode (channels 79–86), left fronto-polar strip electrode (channels 87–94), left fronto-basal strip electrode (channels 95–102). Channels recording from regions that were later surgically removed are marked by bars on the left and right margins of panels d and e.

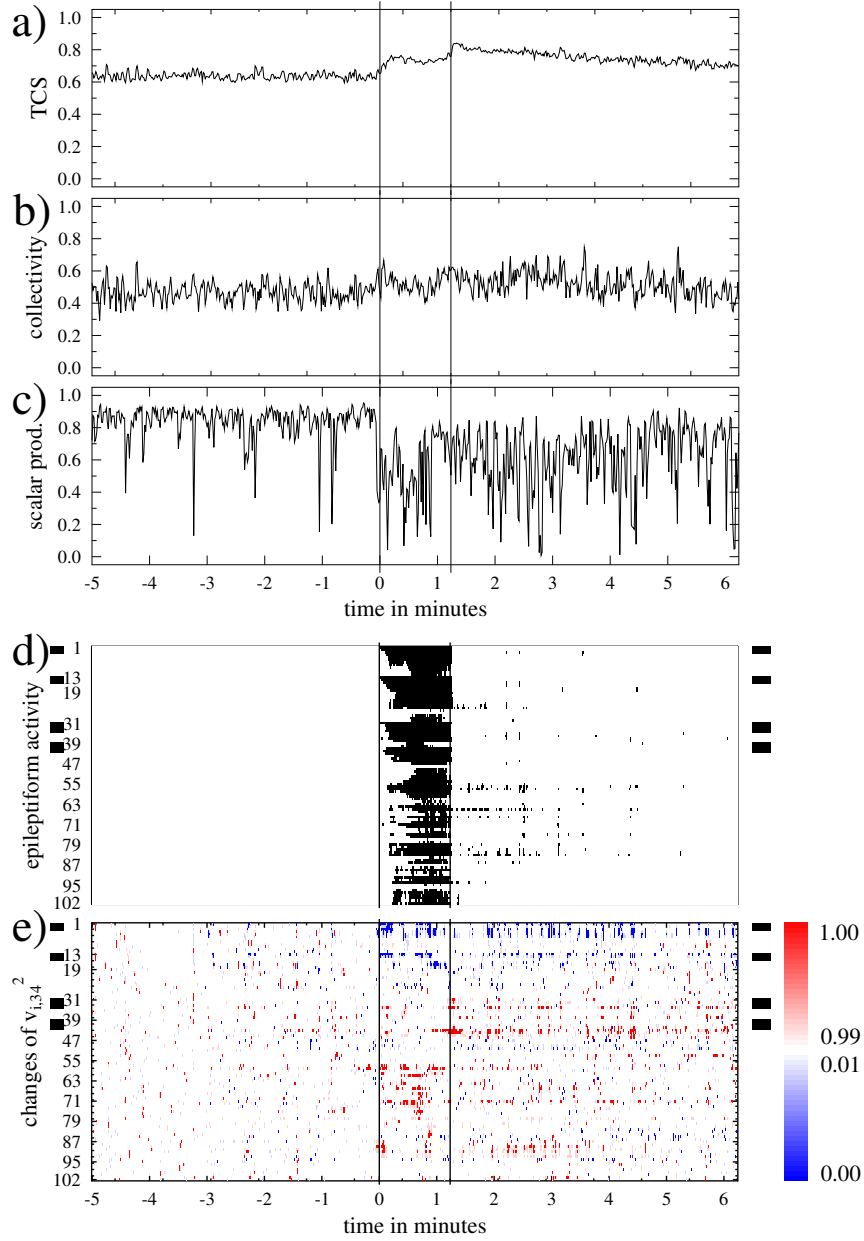


Figure S13: (colour) Same as Fig. S12 but for **CC** based measures for the **first seizure of patient 6** with onset in the *right* temporal lobe. Sequence of iEEG channels from top to bottom: right temporal depth electrode 1 (channels 1–12), right temporal depth electrode 2 (channels 13–18), left temporal depth electrode (channels 19–30), right temporo-polar strip electrode (channels 31–38), right temporo-basal strip electrode (channels 39–46), right temporo-central strip electrode (channels 47–54), right fronto-mesial strip electrode (channels 55–62), right fronto-polar strip electrode (channels 63–70), right fronto-basal strip electrode (channels 71–78), left fronto-mesial strip electrode (channels 79–86), left fronto-polar strip electrode (channels 87–94), left fronto-basal strip electrode (channels 95–102). Channels recording from regions that were later surgically removed are marked by bars on the left and right margins of panels d and e.

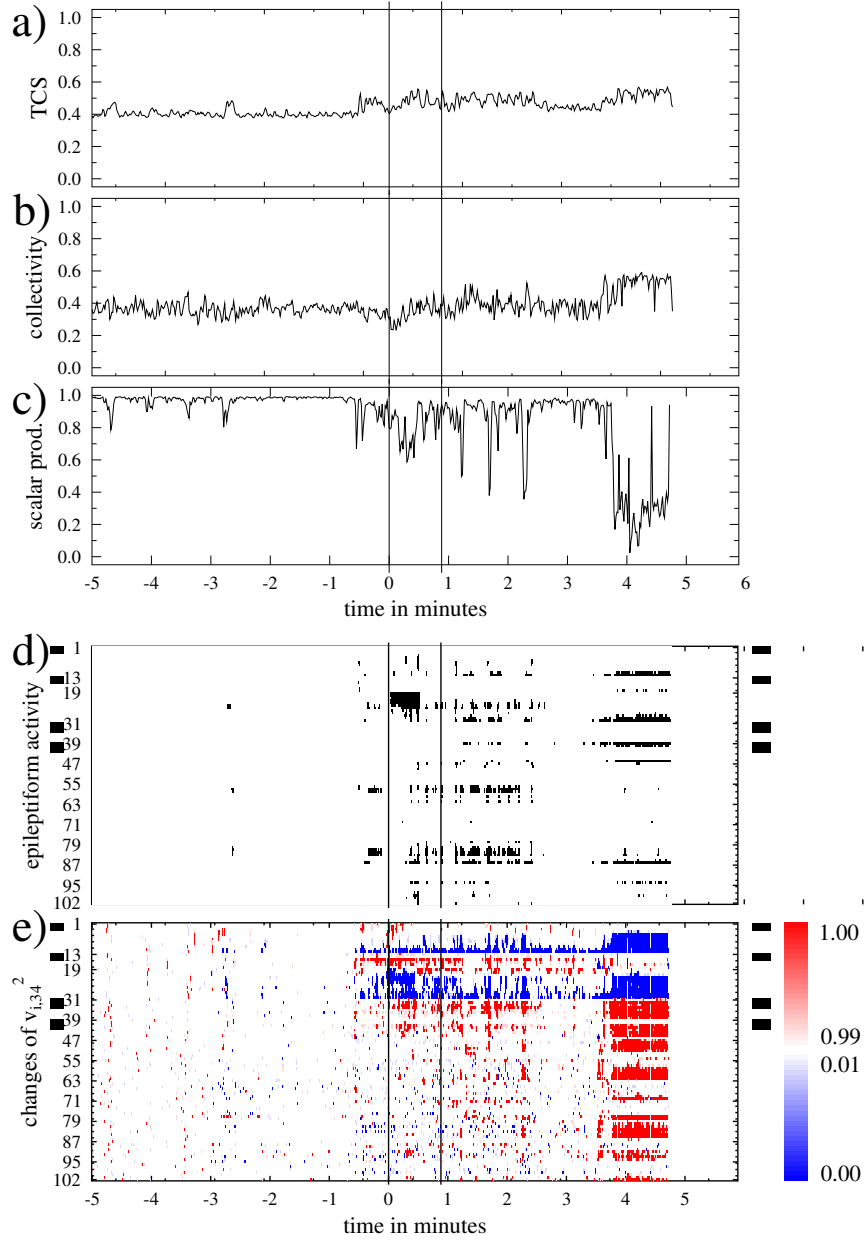


Figure S14: (colour) Same as Fig. S2 but for **SCC** based measures for the **first seizure of patient 6** with onset in the *left* temporal lobe. Sequence of iEEG channels from top to bottom: right temporal depth electrode 1 (channels 1–12), right temporal depth electrode 2 (channels 13–18), left temporal depth electrode (channels 19–30), right temporo-polar strip electrode (channels 31–38), right temporo-basal strip electrode (channels 39–46), right temporo-central strip electrode (channels 47–54), right fronto-mesial strip electrode (channels 55–62), right fronto-polar strip electrode (channels 63–70), right fronto-basal strip electrode (channels 71–78), left fronto-mesial strip electrode (channels 79–86), left fronto-polar strip electrode (channels 87–94), left fronto-basal strip electrode (channels 95–102). Channels recording from regions that were later surgically removed are marked by bars on the left and right margins of panels d and e.

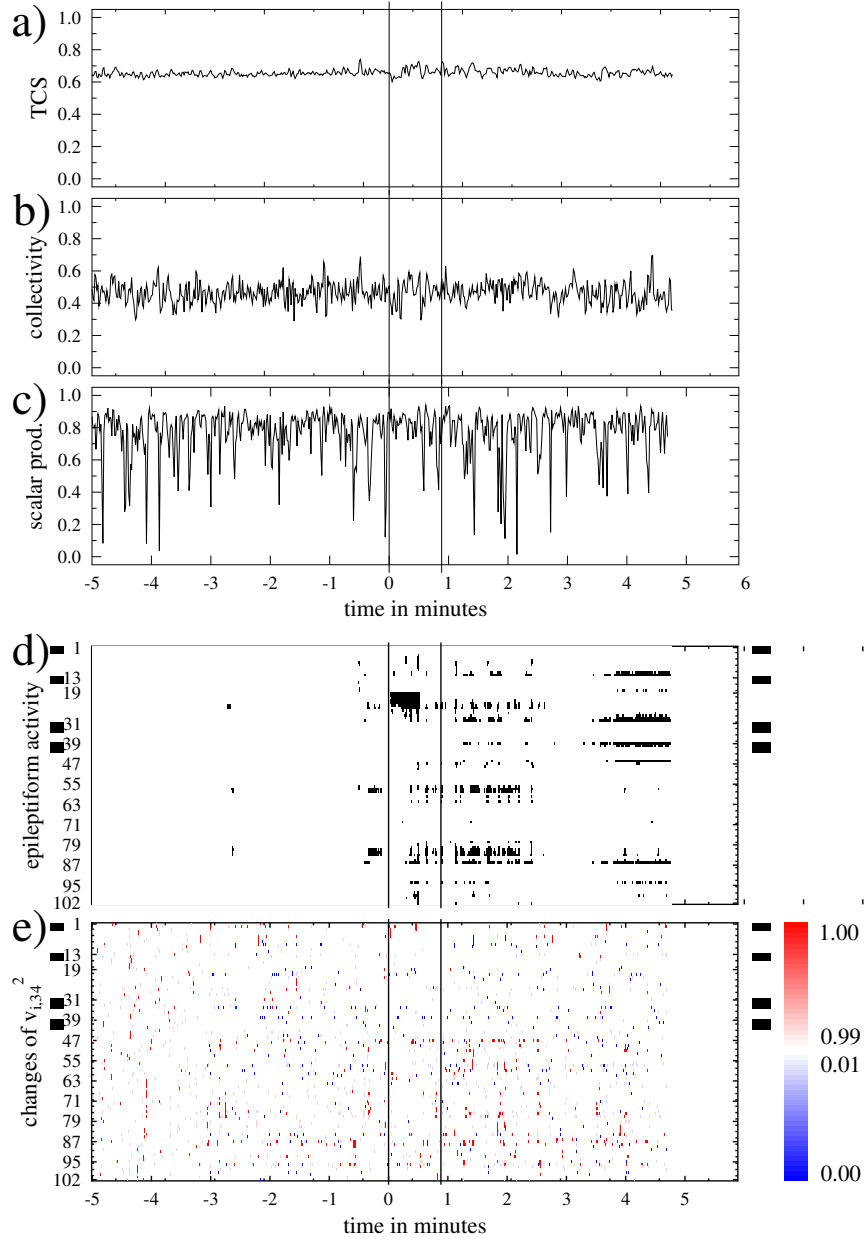


Figure S15: (colour) Same as Fig. S14 but for **CC** based measures for the **first seizure of patient 6** with onset in the *left* temporal lobe. Sequence of iEEG channels from top to bottom: right temporal depth electrode 1 (channels 1–12), right temporal depth electrode 2 (channels 13–18), left temporal depth electrode (channels 19–30), right temporo-polar strip electrode (channels 31–38), right temporo-basal strip electrode (channels 39–46), right temporo-central strip electrode (channels 47–54), right fronto-mesial strip electrode (channels 55–62), right fronto-polar strip electrode (channels 63–70), right fronto-basal strip electrode (channels 71–78), left fronto-mesial strip electrode (channels 79–86), left fronto-polar strip electrode (channels 87–94), left fronto-basal strip electrode (channels 95–102). Channels recording from regions that were later surgically removed are marked by bars on the left and right margins of panels d and e.

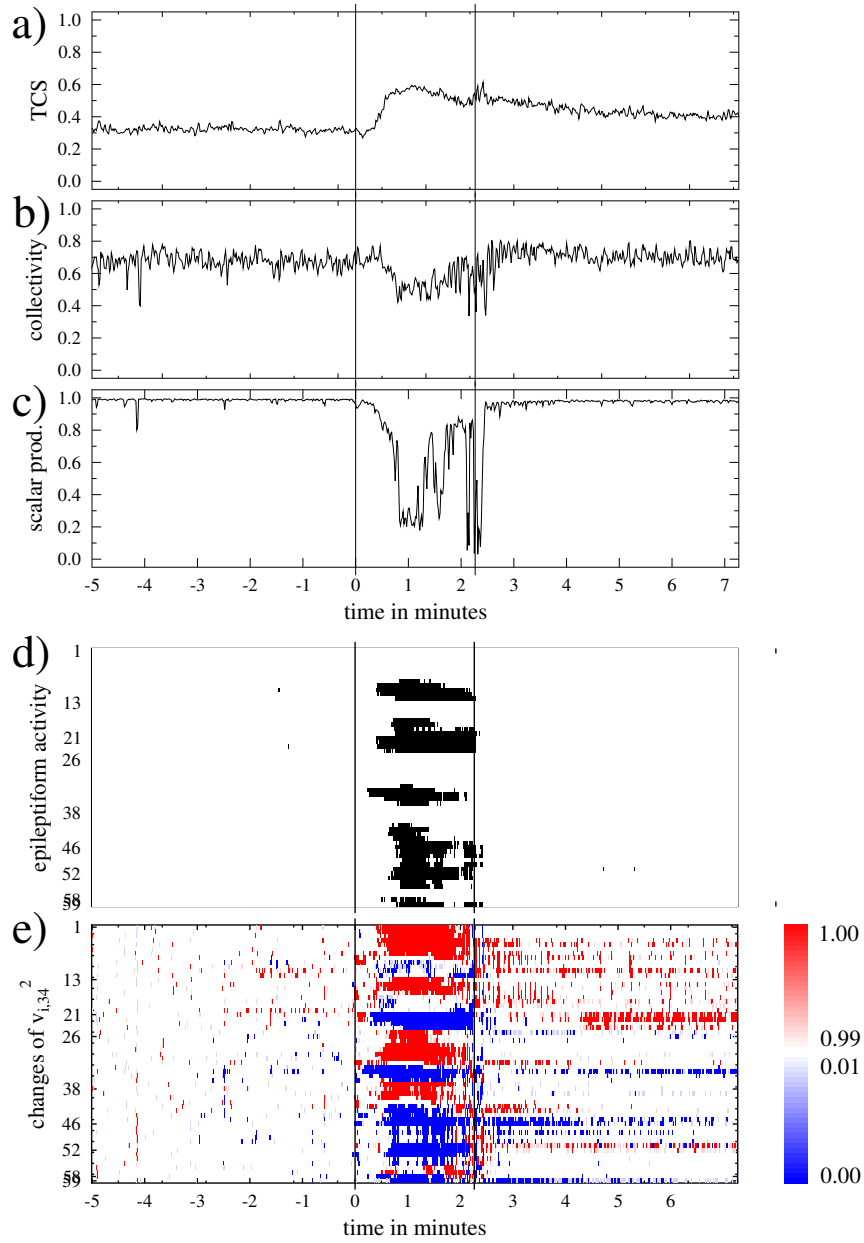


Figure S16: (colour) Same as Fig. S2 but for **SCC** based measures but for the **first seizure of patient 7**. Sequence of iEEG channels from top to bottom: left interhemispheric (channels 1–12), left occipito-temporo-basal (channels 13–20), left temporo-basal (channels 21–24), right interhemispheric (channels 25–36), right occipito-temporo-basal (channels 37–44), right temporo-latero-polar (channels 45–50), right temporo-basal (channels 51–56), right temporo-lateral (channels 57–59)

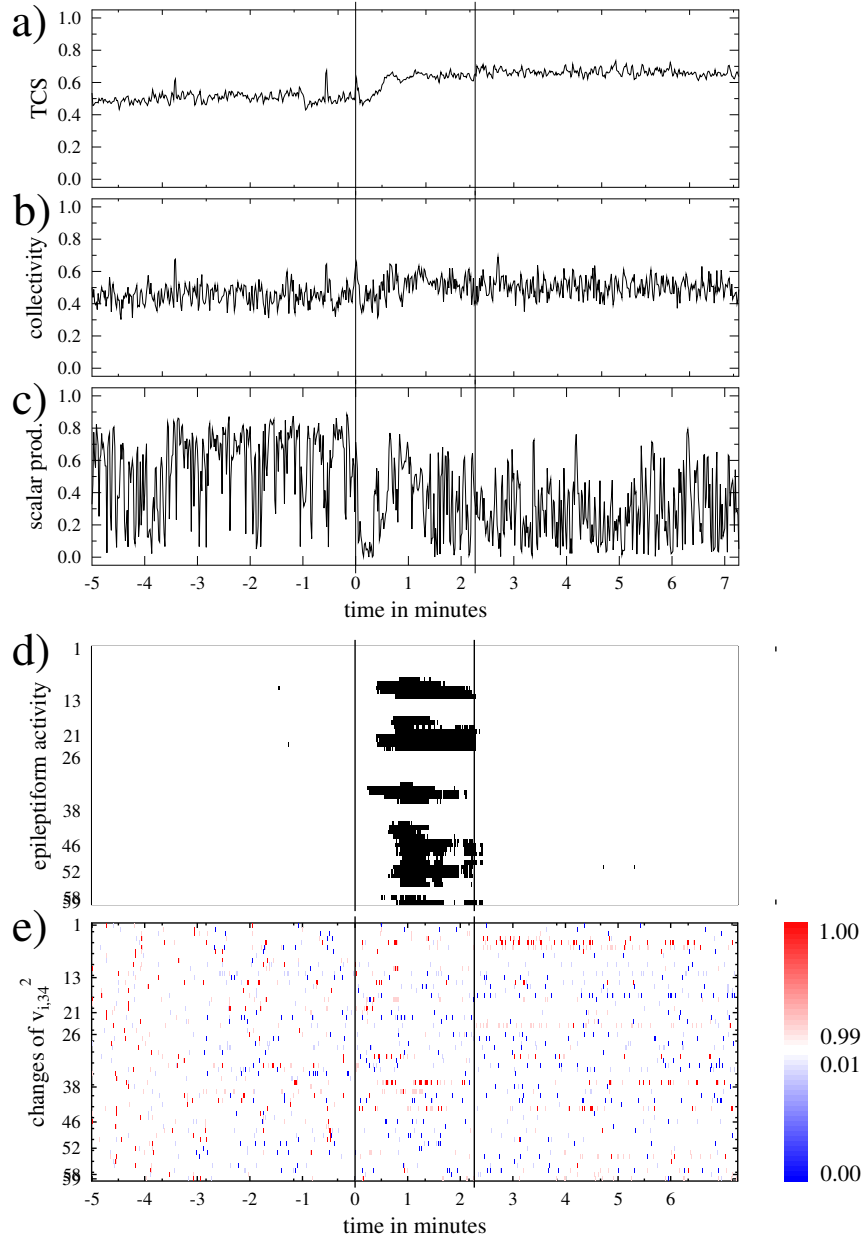


Figure S17: (colour) Same as Fig. S16 but for **CC** based measures for the **first seizure of patient 7**. Sequence of iEEG channels from top to bottom: left interhemispheric (channels 1–12), left occipito-temporo-basal (channels 13–20), left temporo-basal (channels 21–24), right interhemispheric (channels 25–36), right occipito-temporo-basal (channels 37–44), right temporo-latero-polar (channels 45–50), right temporo-basal (channels 51–56), right temporo-lateral (channels 57–59)

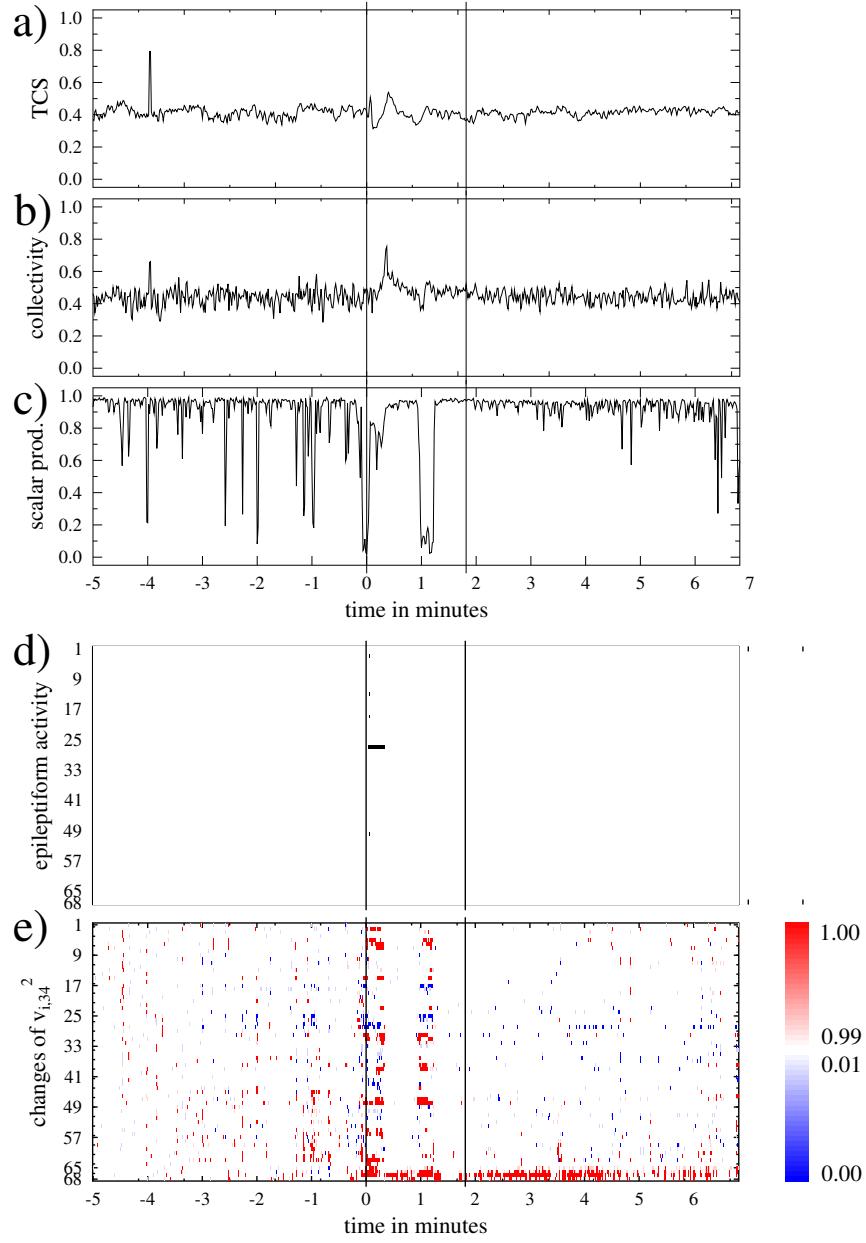


Figure S18: (colour) Same as Fig. S2 but for **SCC** based measures but for the **first seizure of patient 8**. Sequence of iEEG channels from top to bottom: depth electrode in the left parietal lobe (channels 1–4), grid electrode placed over the left parietal lobe (channels 5–68).

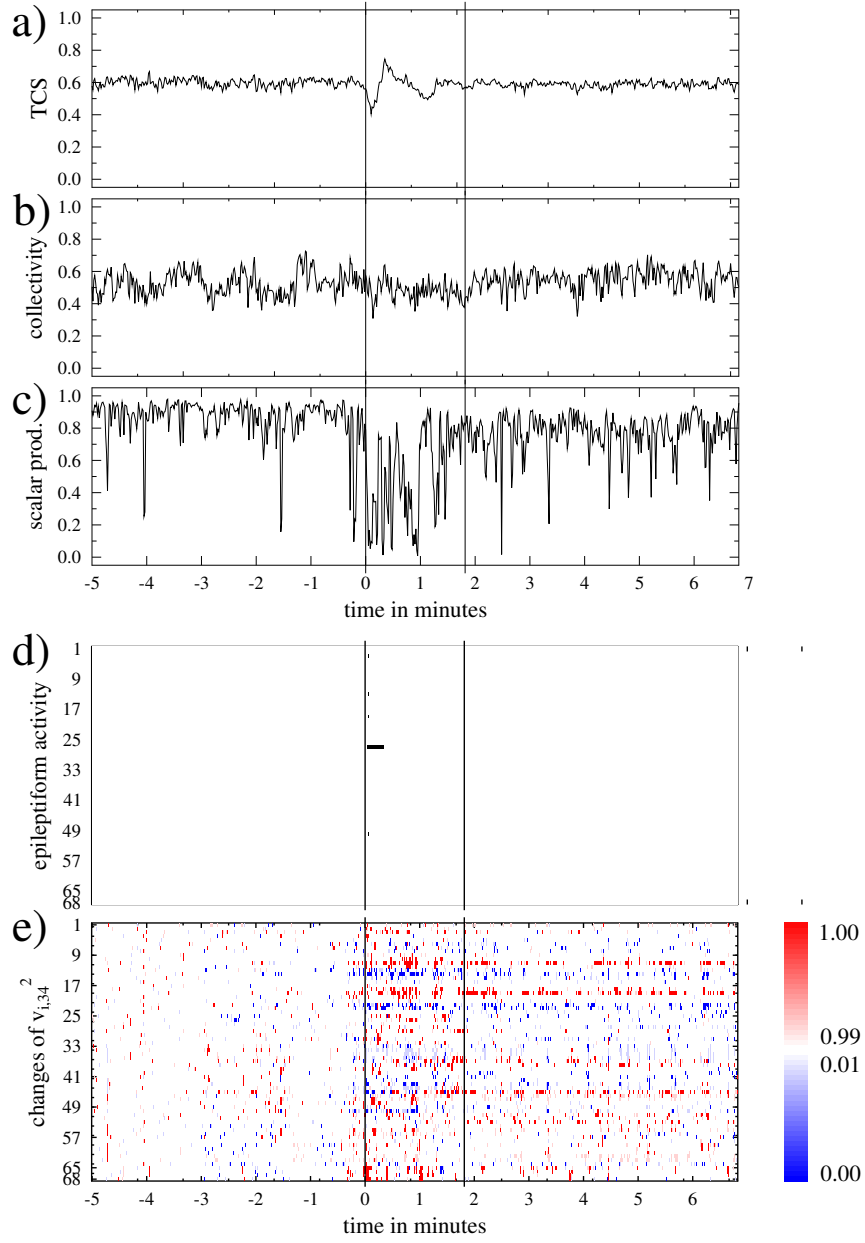


Figure S19: (colour) Same as Fig. S2 but for **CC** based measures for the **first seizure of patient 8**. Sequence of iEEG channels from top to bottom: depth electrode in the left parietal lobe (channels 1–4), grid electrode placed over the left parietal lobe (channels 5–68).

References

- Allefeld, C., Bialonski, S., 2007. Detecting synchronization clusters in multivariate time series via coarse-graining of Markov chains. *Phys. Rev. E* 76, 066207.
- Allefeld, C., Müller, M., Kurths, J., 2007. Eigenvalue decomposition as a generalized synchronization cluster analysis. *Int. J. Bifurcat. Chaos* 17, 3493–3497.
- Bialonski, S., Lehnertz, K., 2006. Identifying phase synchronization clusters in spatially extended dynamical systems. *Phys. Rev. E* 74, 051909.
- Jolliffe, I. T., 1986. *Principal Component Analysis*. Springer, Berlin.
- Müller, M., Baier, G., Rummel, C., Schindler, K., 2008a. Estimating the strength of genuine and random correlations in non-stationary multivariate time series. *Eur. Phys. Lett.* 84, 10009.
- Müller, M., Baier, G., Rummel, C., Schindler, K., Stephani, U., 2008b. A multivariate approach to correlation analysis based on random matrix theory. In: Schulze-Bonhage, A., Timmer, J., Schelter, B. (Eds.), *Seizure Prediction in Epilepsy: From Basic Mechanisms to Clinical Applications*. Wiley, pp. 209–226.
- Plerou, V., Gopikrishnan, P., Rosenow, B., Nunes Amaral, L. A., Guhr, T., Stanley, H. E., 2002. Random matrix approach to cross correlations in financial data. *Phys. Rev. E* 65, 066126.
- Rummel, C., 2008. Quantification of intra- and inter-cluster relations in non-stationary and noisy data. *Phys. Rev. E* 77, 016708.
- Rummel, C., Baier, G., Müller, M., 2007. Automated detection of time-dependent cross-correlation clusters in nonstationary time series. *Europhys. Lett.* 80, 68004.
- Rummel, C., Müller, M., Baier, G., Amor, F., Schindler, K., 2010. Analyzing spatio-temporal patterns of genuine cross-correlations. *J. Neurosci. Meth.* 191, 94–100.
- Rummel, C., Müller, M., Schindler, K., 2008. Data-driven estimates of the number of clusters in multivariate time series. *Phys. Rev. E* 78, 066703.
- Schindler, K., Amor, F., Gast, H., Müller, M., Stibal, A., Mariani, L., Rummel, C., 2010. Peri-ictal correlation dynamics of high frequency (80–200Hz) intracranial EEG. *Epilepsy Res.* 89, 72–81.
- Schindler, K., Elger, C. E., Lehnertz, K., 2007a. Increasing synchronization may promote seizure termination: Evidence from status epilepticus. *Clin. Neurophysiol.* 118, 1955–1968.
- Schindler, K., Leung, H., Elger, C. E., Lehnertz, K., 2007b. Assessing seizure dynamics by analysing the correlation structure of multichannel intracranial EEG. *Brain* 130, 65–77.